# A Microwave Retrieval Algorithm of Above Cloud Electric Fields

Michael J Peterson[1,*], Chuntao Liu[2], Douglas Mach[3], Wiebke Deierling[4], Christina Kalb[4]

1. Department of Atmospheric Sciences, University of Utah
2. Department of Physical and Environmental Sciences, Texas A & M University - Corpus Christi
3. Global Hydrology and Climate Center, University of Alabama, Huntsville
4. National Center for Atmospheric Research

**ABSTRACT:** A microwave retrieval algorithm of above cloud electric fields is developed using coincident high-altitude NASA ER-2 aircraft passive microwave and electric field observations over the course of four different field campaigns in North and South America. Such a microwave retrieval algorithm could be a useful tool for studying the Global Electric Circuit if it could be applied to a global satellite microwave dataset. The purpose of this study is to assess the performance of this algorithm and identify potential challenges to applying it to a global satellite passive microwave dataset and possible avenues for algorithm development and improvement. Over land, the algorithm is shown to estimate electric fields above convective clouds to within a factor of two of observations 53% of the time for weakly electrified shower clouds and 70% of the time for convective and significantly electrified (> 100 V/m) shower clouds using only 85 GHz passive microwave observations.

## INTRODUCTION

The Global Electric Circuit (GEC) is an important part of Earth-atmosphere system that describes the interactions of its various electrical phenomena [Williams et al., 2009]. Charge accumulation within electrified clouds serves as a current source for the direct current branch of the GEC wherein cloud charge interacts with the highly-conducting ionosphere above to maintain its electrical potential of around 240 kV relative to the ground [Wilson, 1924; Alderman and Williams, 1996]. These upward currents from electrified clouds [Wilson currents, Wilson, 1920] are balanced by fair weather return currents across the globe.

The GEC has been widely studied over the past century, beginning in the 1920's when two different research vessels, the Carnegie and the Maud, traversed the globe taking observations of the diurnal cycle of fair-weather electric fields (the Carnegie Curve), which were shown to closely relate to thunderstorm activity [Whipple and Scrase, 1936]. Since then, many studies have used more modern techniques to explore this relationship [Blakeslee et al., 1999; Bailey et al., 2007; Williams, 2009; Liu et al., 2010;

* Contact information: Michael Peterson, University of Utah, 135 S 1460 E RM 819 (WBB), Salt Lake City, UT 84112
Email: michael.j.peterson@utah.edu

Mach et al., 2009, 2010, 2011]. However, these studies only provide an ensemble view of global electricity and are only applicable for approximating the GEC on annual and seasonal timescales, and generally do not sufficiently describe how different types of storms and electrified shower clouds contribute to the GEC.

The most direct method of examining the Wilson Currents that drive the GEC is through high-altitude aircraft electric field observations. However, these observations are limited to a relatively small number of field campaigns in a few key regions of the world. A global dataset of high-altitude electric fields would be a valuable tool for studying the GEC, but would also be impractical to obtain directly by research aircraft or balloon. Another approach would be to estimate high-altitude electric fields from common global satellite observations. To this end, a high-altitude electric field retrieval algorithm has been created from NASA ER-2 overflight data that uses passive microwave observations to characterize the electrical activity of thunderstorms and electrified shower clouds. While developed using high-altitude aircraft observations, such an algorithm could be refined for use with Tropical Rainfall Measuring Mission (TRMM) or Global Precipitation Mission (GPM) observations to provide a unique method for examining the GEC.

## DATA AND METHODOLOGY

The basic premise of this algorithm that allows it to estimate electric fields from passive microwave observations is that the primary source of charge in electrified clouds is considered to be local cloud ice processes. Supercooled liquid water, a necessary component for the non-inductive charging mechanism [Reynolds et al., 1957; Takahashi, 1978; Jayaratne et al., 1983; Saunders et al., 1991; Saunders and Peck, 1998; Takahashi and Miyawaki, 2002; Mansell et al., 2005], is assumed to be present in sufficient quantities as to not inhibit charging, and advective sources of charge are not considered in this version. Following this assumption, the amount of charge generated by a particular cloud is dependent on the frequency of collisions between ice particles, which then depends on the concentration of ice particles within the cloud. Since column ice-water path has been shown to be directly related to passive microwave brightness temperatures at 37 GHz and 85 GHz [Vivekanandan et al., 1991], it may therefore be possible to infer charging from passive microwave observations.

The algorithm estimates electric fields above electrified clouds in two processing steps. In the first step, a proxy variable for the net electric field vector at a given location is computed by integrating Coulomb's Law across a subdomain of nearby microwave pixels. This is done for each observation in the microwave dataset to obtain proxy electric field vectors for each data point. In the second step of processing, the magnitudes of the microwave proxy electric field vectors are tuned to observations using a statistical model, which can be compared to observations. Technical details about the electric field estimation process, the calculations performed within the algorithm, the theoretical basis for each equation, and the caveats and additional assumptions involved will be discussed in Peterson et al. [2014]. However, some of the most significant caveats and assumptions are: the amount of ice in the mixed-phase region is directly related the tot total column ice water path; the charge structure of electrified clouds follows the tri-pole model [Williams et al., 1989] where the upper positive charge layer is of primary importance to Wilson current generation; and the height of this charge layer is allowed to fluctuate based on the convective intensity of the storm region using a rough lookup table derived from coincident TRMM [Kummerow et

al., 1998] PR and TMI observations. It is clear from this list that the algorithm was designed with electrified convective clouds in mind, and therefore it may not characterize electrified stratiform or anvil clouds properly.

The statistical models employed by the algorithm to convert from proxy electric field magnitudes to real-world electric fields were created using the algorithm basis dataset, which consists of NASA ER-2 Advanced Microwave Precipitation Radiometer [AMPR, Spencer et al., 1994] passive microwave brightness temperatures and Lightning Instrument Package [LIP, Bateman et al., 2007] electric fields taken over the course of numerous ER-2 flights during four different field campaigns, including the third and the fourth Convection and Moisture Experiments [CAMEX-3, CAMEX-4: Kakar et al., 2006], the Tropical Cloud Systems and Processes mission [TCSP: Halverson et al., 2007], and the Tropical Rainfall Measuring Mission Large-scale Biosphere Atmosphere field campaign [TRMM-LBA: Halverson and Rickenbach, 2002]. The use of AMPR and LIP observations as the algorithm basis dataset introduces additional caveats, which include: the open ocean surface appears similar to intense convection to AMPR at 37 GHz since it is a total power radiometer; the width of the AMPR swath is only 30-40 km across at ground level and does not always capture the entire storm; despite performing quality on the LIP dataset, lightning artifacts are still present. This dataset is also used for validation of the algorithm to determine where is performs well and where it needs improvement.

**RESULTS**

A comparison between algorithm-derived high-altitude electric field estimates using 37 GHz and 85 GHz AMPR observations and LIP electric field observations over land is shown using two-dimensional cumulative histograms in Figure 1. Additionally, 1:1 lines indicating where the algorithm estimates match observations and plots of the first through third quartiles of LIP electric field observations for varying algorithm estimated values are overlain. While the contours and quartile plots for the 37 GHz estimate are distributed well throughout the figure, both indicators of algorithm performance are concentrated along the 1:1 line for the 85 GHz estimate. Table 1 examines the performance of the algorithm by examining how often the algorithm produces estimates that are within a factor of two of observations. Estimates based on 85 GHz observations fall within this threshold between at least 53% of the time over land and the algorithm has a nearly 70% success rate for clouds with significant observed electric fields (> 100 V/m) and convective clouds. The success rate of the 85 GHz routine can be as low as 13% for marine clouds, but improves to 42% to 55% for marine clouds with strong observed electric fields.

Algorithm errors can generally be divided into two groups: false alarm cases and missed event cases. False alarm cases, which fall to the right of the 1:1 line in Figure 1, occur when the algorithm predicts strong electric fields, but much weaker electric fields are observed. False alarms typically result from deficiencies in the algorithm – particularly with stratiform cloud regions. False alarm cases account for most of the error in the 85 GHz estimates, including 83% marine shower cloud observations. Missed event cases, on the other hand, occur when the algorithm produces electric field estimates that are much lower than observations. Missed events often occur when electrified clouds are not entirely contained within the limited AMPR swath. Since the LIP detects eclectic fields from any nearby electrified cloud and is not limited to a narrow swath, large clouds or clouds that the aircraft is not able to fly over will be detected by the LIP but not AMPR, leading to missed events. Missed events are also created by lightning artifacts

within the LIP record. Missed events are less common than false alarms for 85 GHz estimates, but still constitute a significant source of error, particularly for shower clouds with strong electric fields.

Figure 2 shows how the algorithm electric field estimates compare observations for an individual case. In this Amazon convection case, the ER-2 flies over two separate convective features without large regions of nearby stratiform precipitation that are well bounded by the AMPR swath. AMPR 37 GHz (a and c) and 85 GHz (b and d) brightness temperatures and estimated electric fields are shown along with comparisons of flight-track electrical field estimates and LIP observations. Electric field estimates over the convective features from both frequencies are characterized by a close-contour maximum over the stronger eastern feature and a plateau extending across the clear air between the features to the weaker western feature. The flight path takes the ER-2 directly across this plateau and alongside the electric field estimate peak. LIP observations follow this pattern, but are most similar to the 85 GHz estimates, which approximate the general shape, timing, and strength of the event to within a few percent throughout the overflight.

In contrast to Figure 2, which showed a case where the algorithm performed well at 85 GHz, Figure 3 shows an example false alarm case. In this oceanic case, the ER-2 crossed over a mature Mesoscale Convective System (MCS) from east to west (Figure 3a). This case includes some missing AMPR data, but these datapoints are not included in the electric field calculations. The MCS is larger than the AMPR swath width, resulting in an unrealistic closed contour electric field estimate pattern over the storm. Electric field estimates reach their maximum value well behind the convective leading line in the stratiform region. Electric field estimates along the flight track are compared with LIP observations in Figure 3b. As the aircraft approaches the storm, electric field observations and estimates increase at roughly the same rate, reaching a maximum value over the convective line of 150 V/m. As the aircraft crosses the transition zone into the stratiform region, however, estimates and observations begin to diverge. While observations quickly decrease to below 100 V/m 10 km behind the convective peak, electric field estimates remain high, and even continue to increase. By the end of the overflight, estimated electric fields of 100 V/m are recorded, even though observed electric fields are virtually 0 V/m.

The algorithm significantly overestimates stratiform electric fields because of the assumptions it makes about the structure and source of charge within the cloud layer. While charge in convective clouds is often lofted by strong updrafts to high levels, often resulting in a typical tri-pole charge structure spanning the entire cloud layer, charge within stratiform regions accumulates in a series of horizontally extensive charge layers of alternating polarity [Schuur and Rutledge 2000]. Since stratiform clouds lack the intense updrafts that lead to the strong charge separation in convective regions, the transport of charge from other parts of the storm is an important source of charge for stratiform clouds. A lack of intense updrafts also allows strong screening layers to form above the cloud, reducing the electric fields observed above stratiform clouds.

## CONCLUSION

A microwave retrieval algorithm has been developed to estimate electric fields above electrified clouds from 37 GHz and 85 GHz passive microwave observations and validated using high-altitude aircraft observations. The algorithm was shown to compute electric fields above convective storms using 85 GHz

observations with a reasonable amount of accuracy overall and for individual cases. The algorithm did not perform as well with 37 GHz observations and in estimating electric fields over stratiform cloud regions. These results suggest that this estimation method is feasible, but further refinement is needed before it can be applied to a global satellite dataset.

## ACKNOWLEDGMENTS

This research was supported by NASA PMM grant NNX13AQ70G under the direction of Dr. Ramesh Kakar and NASA Grant NNX08AK28G under the direction of Dr. Erich Stocker. AMPR data were obtained from the NASA EOSDIS Global Hydrology Resource Center DAAC, Huntsville, AL.

## REFERENCES

Alderman, E. J., and E. R. Williams, 1996: Seasonal variation of the global electric circuit. *J. Geophys. Res.,* **101**, D23, 29,679-29,688.

Bailey, J. C., R. J. Blakeslee, D. E. Buechler, and H. J. Christian, 2007: Diurnal lightning distributions as observed by the Optical Transient Detector (OTD) and the Lightning Imaging Sensor (LIS), paper presented at 13th International Conference on Atmospheric Electricity, *Int. Comm. on Atmos. Electr.*, Beijing.

Bateman, M. G., M. F. Stewart, R. J. Blakeslee, S. J. Podgorny, H. J. Christian, D. M. Mach, J. C. Bailey, and D. Daskar, 2007: A low‐noise, microprocessor‐controlled, internally digitizing rotating‐vane electric field mill for airborne platforms, *J. Atmos. Oceanic Technol.,* **24**, 1245–1255, doi:10.1175/JTECH2039.1.

Blakeslee, R. J., et al., 1999: Diurnal lightning distribution as observed by the Optical Transient Detector (OTD), in 11th International Conference on Atmospheric Electricity, *NASA Conf. Publ.*, NASA/CP‐1999‐209261, 742–745.

Halverson, J., M. Black, S. Braun, D. Cecil, M. Goodman, A. Heymsfield, G. Heymsfield, R. Hood, T. Krishnamurti, G. McFarquhar, M. J. Mahoney, J. Molinari, R. Rogers, J. Turk, C. Velden, D.-L. Zhang, E. Zipser, and R. Kakar, 2007: NASA's tropical cloud systems and processes experiment. *Bull. Amer. Meteor. Soc.*, **88,** 6, 867-882.

Jayaratne, E. R., C. P. R. Saunders, and J. Hallet, 1983: Laboratory studies of the charging of soft hail during ice crystal interactions. *Quart. J. Roy. Meteor. Soc.,* **109,** 609–630.

Kaker, R., M. Goodman, R. Hood, and A. Guillory, 2006: Overview of the convection and moisture experiment (CAMEX). *J. Atmos. Sci.*, **63,** 5-18.

Kummerow, C., W. Barnes, T. Kozu, J. Shiue, and J. Simpson, 1998: The Tropical Rainfall Measuring Mission (TRMM) sensor package. *J. Atmos. Oceanic Technol.*, **15**, 809–817.

Liu, C., E. Williams, E. J. Zipser, and G. Burns, 2010: Diurnal variations of global thunderstorms and electrified shower clouds and their contribution to the global electrical circuit, *J. Atmos. Sci.*, **67**, 309–323, doi:10.1175/2009JAS3248.1.

------, D. Cecil, and E. J. Zipser, 2012: Relationships between lightning flash rates and radar reflectivity vertical structures in thunderstorms over the tropics and subtropics. *J. Geophys. Res*., **117,** 2156-2202.

Mach, D. M., R. J. Blakeslee, M. G. Bateman, and J. C. Bailey, 2009: Electric fields, conductivity, and estimated currents from aircraft overflights of electrified clouds. *J. Geophys. Res.*, **114**, D10204, doi:10.1029/2008JD011495.

------, ------, ------, and ------, 2010: Comparisons of total currents based on storm location, polarity, and flash rates derived from high-altitude aircraft overflights, *J. Geophys. Res.*, **115**, D03201.

------, ------, and ------, 2011: Global electric circuit implications of combined aircraft storm electric current measurements and satellite-based diurnal lightning statistics, *J. Geophys. Res.*, **116**, D05201, doi:10.1029/2010JD014462.

Mansell, E. R., D. R. MacGorman, C. L. Ziegler, and J. M. Straka, 2005: Charge structure and lightning sensitivity in a simulated multicell thunderstorm. *J. Geophys. Res.*, **110**, D12101, doi:10.1029/2004JD005287.

Marshall, J. S., and S. Radhakant, 1978: Radar precipitation maps as lightning indicators. *J. Appl. Meteorol.*, **17,** 206-212.

Peterson, M. J. 2011: Satellite and ground based observations of lightning flashes in the stratiform and anvil regions of convective systems. *M.S. thesis*, 139 pages.

------, C. Liu, D. Mach, W. Deierling, and C. Kalb, 2014: A method of estimating electric fields above electrified clouds from passive microwave observations. *J. Atmos. Oceanic Tech.,* to be submitted.

Saunders, C. P. R., W. D. Keith, and R. P. Mitzeva, 1991: The effect of liquid water content on

thunderstorm charging. *J. Geophys. Res.,* **96,** 11,007–11,017.

------, and S. L. Peck, 1998: Laboratory studies of the influence of the rime accretion rate on charge transfer during crystal/graupel collisions. *J. Geophys. Res.*, **103,** D12, 13,949– 13,956.

Schuur, T. J., and S. A. Rutledge, 2000: Electrification of stratiform regions in mesoscale convective systems. Part II: Two-dimensional numerical model simulations of a symmetric MCS. *J. Atmos. Sci.*, **57,** 1983-2006.

Spencer, R. W., H. G. Goodman, and R. E. Hood, 1989: Precipitation retrieval over land and ocean with the SSM/I: Identification and characteristics of the scattering signal. *J. Atmos. Oceanic Tech.*, **6,** 254-273.

------, Hood, R.E., LaFontaine, F.J., Smith, E.A., Platt, R., Galliano, J., Griffin, V.L., and E. Lobl, 1994: High Resolution Imaging of Rain Systems with the Advanced Microwave Precipitation Radiometer, *J. of Atmos. and Ocean. Tech.*, **11,** 4, 849-857.

------, Hood, R.E., LaFontaine, F.J., Smith, E.A., Platt, R., Galliano, J., Griffin, V.L., and E. Lobl, 1994: High Resolution Imaging of Rain Systems with the Advanced Microwave Precipitation Radiometer, *J. of Atmos. and Ocean. Tech.*, **11,** 4, 849-857.

Takahashi, T., 1978: Riming electrification as a charge generation mechanism in thunderstorms. *J. Atmos. Sci.,* **35,** 1536–1548.

------, and K. Miyawaki, 2002: Reexamination of riming electrification in a wind tunnel. *J. Atmos. Sci.,* **59**, 5, 1018– 1025.

Reynolds, S. E., M. Brook, and M. F. Gourley, 1957: Thunderstorm charge separation. *J. Meteorol.*, **14,** 5, 163–178.

Vivekanandan, J., J. Turk, V. N. Bringi, 1991: Ice Water Path Estimation and Characterization Using Passive Microwave Radiometry. *J. Appl. Meteor.*, **30**, 1407–1421.

Whipple, F. J. W., and F. J. Scrase, 1936: Point-discharge in the electric field of the Earth, *Geophys. Mem.,* 8(68), 1–20.

Williams, E. R., 1989: The tripole structure of thunderstorms, *J. Geophys. Res.*, **94**, 13,151-13,167.

------: The global electrical circuit: A review, *Atmos. Res.*, **91**(2–4), 140–152,

doi:10.1016/j.atmosres.2008.05.018.

Wilson, C.T. R., 1920: Investigation on lightning discharges and on the electric field of thunderstorms. *Phil. Trans. Roy. Soc. Ser. A.,* **221**, 73-115.

------, 1924: The electric field of a thundercloud and some of its effects, *Proc. Phys. Soc. London*, **37**(1), 32D– 37D.

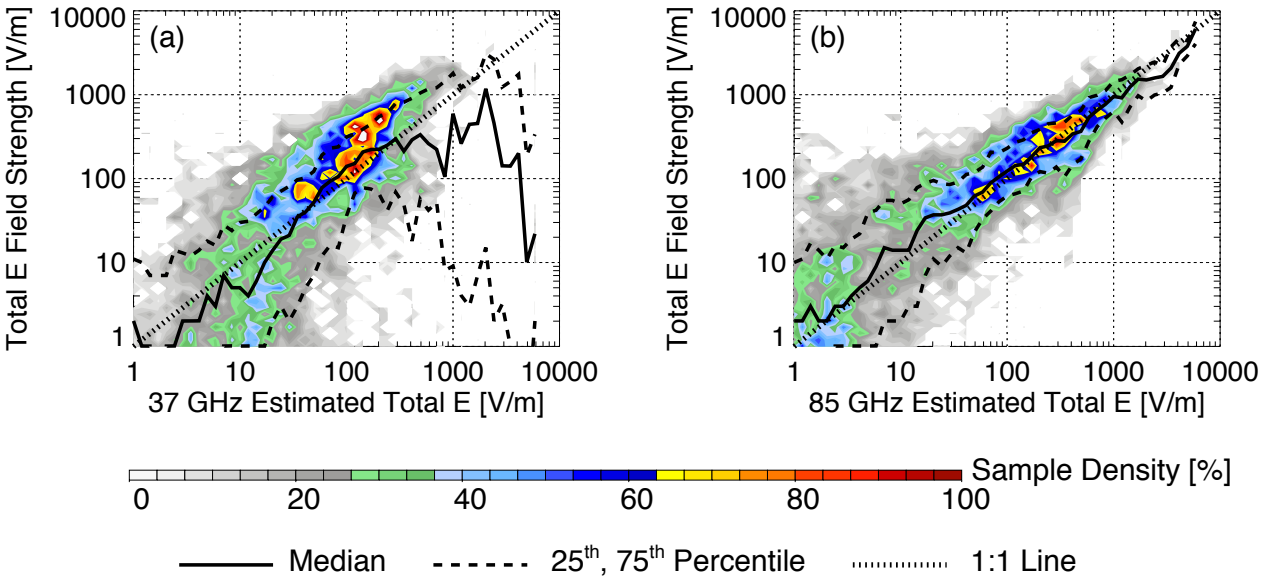


**Figure 1**. Cumulative two-dimensional histograms of 37 GHz (a) and 85 GHz (b) estimated electric field strengths and observed electric fields over land. Quartile plots for various estimated electric field strengths and 1:1 line are overlain.

Table 1 Overall performance of the algorithm using 85 GHz microwave observations

| | Median \|Error\| | \|Error\| < 100% | Error < -100% | Error > 100% |
|---|---|---|---|---|
| *Land* | | | | |
| Shower clouds | 87.8 % | 53.1 % | 12.6 % | 34.3 % |
| > 100 V/m | 56.1 % | 68.2 % | 17.5 % | 14.4 % |
| Convection | 57.5 % | 68.6 % | 7.2 % | 24.2 % |
| > 100 V/m | 56.2 % | 69.5 % | 7.4 % | 23.2 % |
| *Ocean* | | | | |
| Shower clouds | 6,971.1 % | 13.1 % | 4.2 % | 82.6 % |
| > 100 V/m | 84.6 % | 54.9 % | 21.4 % | 23.8 % |
| Convection | 177.3 % | 35.0 % | 9.5 % | 55.6 % |
| > 100 V/m | 127.4 % | 42.3 % | 11.5 % | 46.2 % |

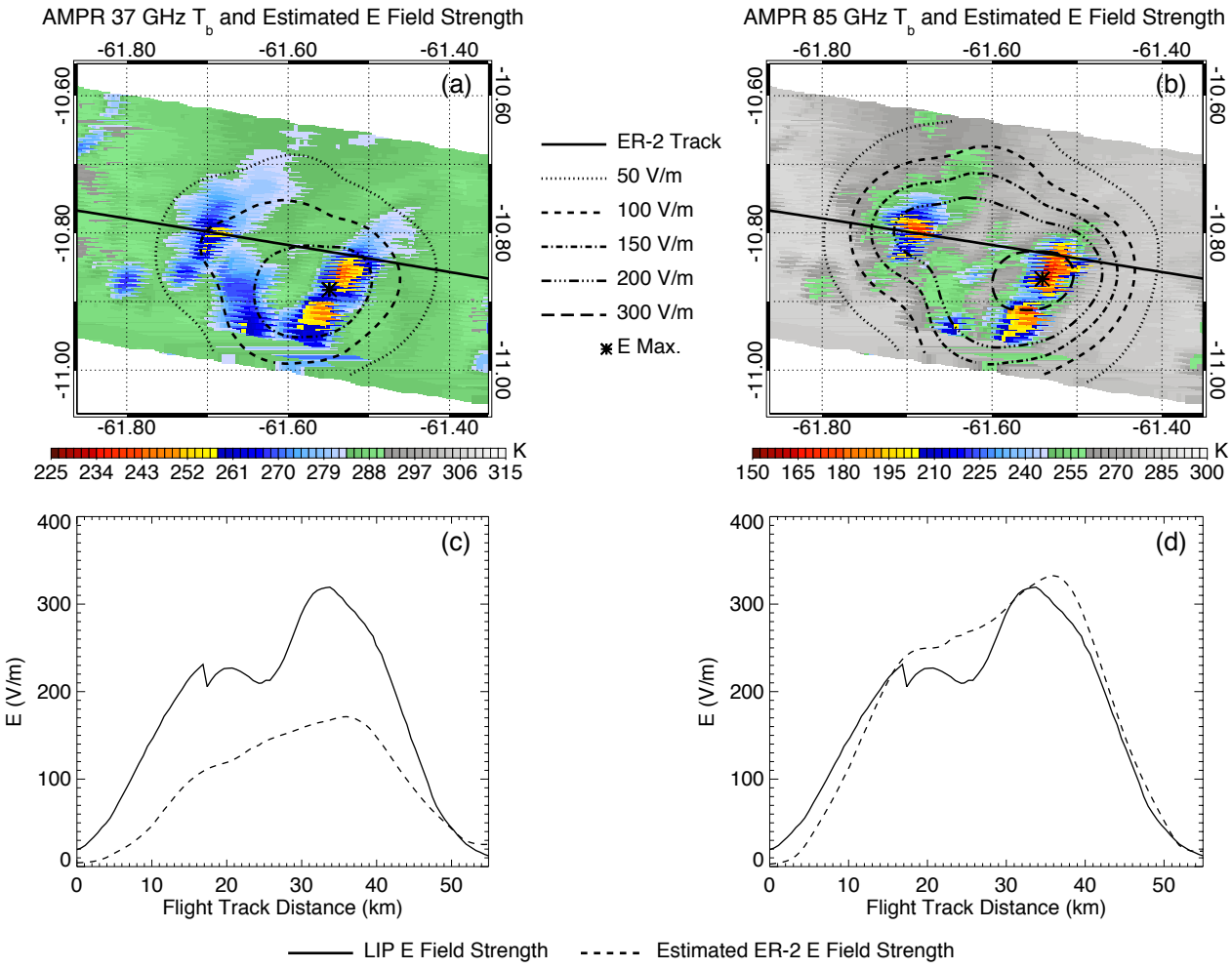


**Figure 2.** AMPR 37 GHz (a) and 85 GHz (b) brightness temperatures (contour) and estimated electric field strengths (line contour) of an overflown storm, and a comparison of observed and 37 GHz (c) and 85 GHz (d) estimated electric field strengths along the ER-2 flight track.

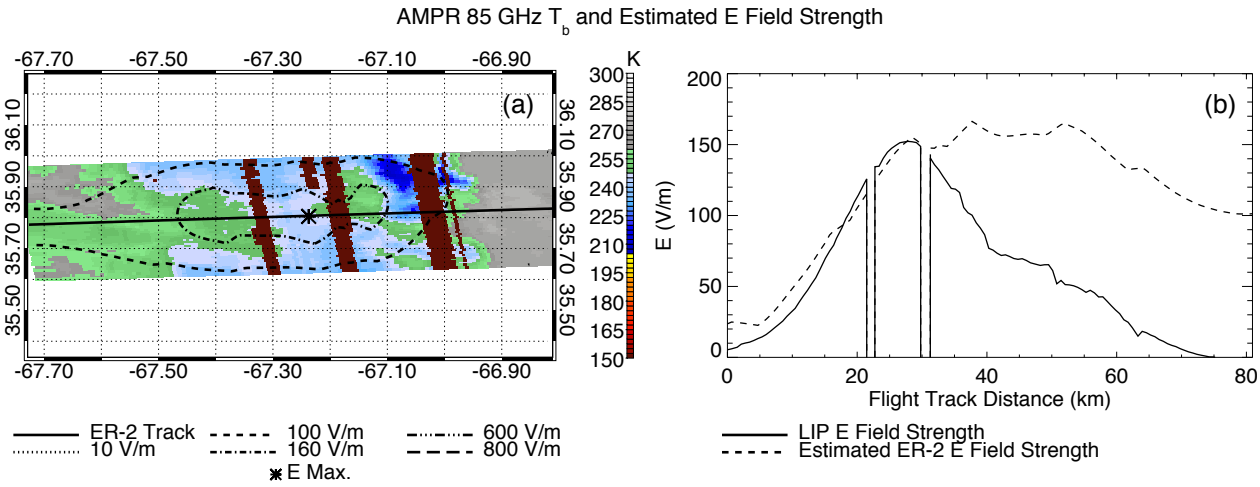


**Figure 3.** AMPR 37 GHz (a) and 85 GHz (b) brightness temperatures (contour) and estimated electric field strengths (line contour) of an overflown MCS, and a comparison of observed and 37 GHz (c) and 85 GHz (d) estimated electric field strengths along the ER-2 flight track.